J. Astrophys. Astr. (2021) 42:19
https://doi.org/10.1007/s12036-021-09692-9

REVIEW

AstroSat: Concept to achievements

S. SEETHA[1,*] and K. KASTURIRANGAN[2]

[1]Raman Research Institute, C.V. Raman Avenue, Bengaluru 560 080, India.
[2]ISRO Headquarters, Antariksh Bhavan, New BEL Road, Bengaluru 560 231, India.
*Corresponding Author. E-mail: venseetha@gmail.com

MS received 16 November 2020; accepted 1 January 2021

Abstract. AstroSat has completed 5 years of successful in-orbit operation on 28 September 2020. AstroSat is ISRO's first Indian multi-wavelength satellite operating as a space Observatory. It is the only satellite which can simultaneously observe in the Far UV and a wide X-ray band from 0.3 to 80 keV using different instruments. This astronomy mission was conceived, following the success of several piggy back astronomy experiments flown earlier on Indian satellites. AstroSat is the result of collaboration between ISRO and several astronomy institutions within India and abroad. There are over 150 refereed publications resulting from data from AstroSat, in addition to Astronomy Telegrams, Circulars and Conference proceedings. This paper provides a brief summary of the evolution of the concept of Astrosat, how it was realized and scientific outcome from this mission.

Keywords. AstroSat—space mission—accretion—X-ray binaries—stars—stellar clusters—galaxies.

1. Introduction

AstroSat is ISRO's first Indian multi-wavelength astronomy satellite being operated as a space observatory. It has completed the design life of five years in orbit on 28 September 2020 and holds promise for further successful operations leading to significant science for at least 5 more years, if not more. It is a satellite having multiple instruments covering both the UV and the X-ray wavebands. This paper provides a brief summary of the environs under which AstroSat was conceptualized, the mode in which it was developed, tested, and is being operated. This paper also gives a glimpse of some of the significant science results from AstroSat.

1.1 *Historical perspective*

India's space program has completed over 50 years since its inception. Space Science experiments have been intertwined with this program, starting with sounding rockets for upper atmospheric studies and X-ray astronomy, moving on to Indian satellites for X-ray and Gamma ray piggyback experiments, finally leading to dedicated missions. In parallel, Tata Institute of Fundamental Research (TIFR) Mumbai has developed a balloon facility at Hyderabad dedicated for conducting science experiments with balloons, which can now be launched to heights of 42 km.

The developments of satellites and launch vehicles have largely been driven by the national priority of space applications for development. However the recognition that these could in turn provide opportunities for new space science experiments was inherent in the vision of the leaders of the space program. This unique approach of developing scientific capabilities without making science as the prime reason for resource investment, gave the Indian Space program a distinct character.

The scientific heritage and the instrumentation capabilities in the country ensured that the space science program matured into an indispensable component of the Indian Space Program.

This article is part of the Special Issue on "AstroSat: Five Years in Orbit".

Published online: 25 May 2021

1.2 *Heritage*

Starting from the 1940s, the foundation for 'space science' began with the experiments to study cosmic rays. This led to development of Balloon fabrication and launch facility by TIFR at Hyderabad that has the capability of carrying a payload of up to several hundred kg to an altitude of 30 to 40 km. This enabled Indian scientists of TIFR and PRL to develop instruments for studies of hard X-rays (>20 keV) from bright X-ray sources. A large number of Balloon experiments for X-ray astronomy studies were conducted from Hyderabad during 1967-1980 resulting in several new and interesting results. In parallel the PRL group initially and later the TIFR group developed instruments for the rocket borne X-ray experiments launched from ISRO's launch facilities at Thumba and Shriharikota in late sixties and up to early eighties for studies of cosmic sources in $\sim$1–10 keV energy range. These provided invaluable training and experience to the Indian scientists for the design and fabrication of the satellite-borne instruments.

Meanwhile, scientists at the Physical Research Laboratory (PRL) at Ahmedabad also conducted research on similar areas of study with emphasis on the solar activity influence on cosmic rays. Further X-ray astronomy experiments from PRL were flown on sounding rockets. Both the teams at TIFR and PRL, also placed a lot of stress on development of instrumentation for these experiments. It is worth pointing out that both the rocket facility at Thumba and the balloon facility at Hyderabad had specific locational advantage for conducting X-ray astronomy studies owing to the low background resulting from the low latitude cut off of the cosmic ray intensity and therefore the reduction of secondary background.

The ground was therefore well prepared when the opportunity arose to fly instruments on board the first Indian satellite 'Aryabhata', and both these groups at PRL and TIFR contributed to two of the astronomy instruments on this satellite.

As the newly created Indian Space Research Organisation (ISRO) gathered momentum, indigenous experimental rockets and satellites provided opportunities for several "piggy back experiments".

The first of these was the Gamma Ray Burst (GRB) experiment developed at ISRO Satellite Centre (ISAC, now UR Rao Satellite Centre (URSC)) flown on the SROSS series of satellites starting in 1987, with a capability of carrying a payload of 5–10 kg. The GRB experiment onboard the SROSS-C2 satellite (Kasturirangan *et al.* 1997) recorded over 50 GRBs, of high signal to noise ratio (Sinha *et al.* 2001). Gamma ray bursts being transient sources with little prior knowledge of the direction, required large field of view instruments to detect the bursts wherever they occurred in the sky. Some of the bursts detected by this experiment were useful for triangulation with other international satellites for localization of the sources.

Although it turned out that this effort was superseded by the launch of the large Compton Gamma Ray Observatory (CGRO) by NASA, it must be said our experiment was an unqualified success.

Encouraged by the success of the GRB instrument, the TIFR and ISAC groups submitted a joint proposal to ISRO for an X-ray Astronomy experiment weighing about 50 kg for launch on an Indian satellite. It was aimed at studies of timing and spectral characteristics of X-ray binaries. This also required inertial pointing of the satellite to specific sources in the sky.

This demanded provision for higher mass and power on the satellite. The development of the Polar Satellite Launch Vehicle (PSLV) by ISRO primarily for remote sensing satellites, enabled the launch of satellites with mass of about 1000 kg into a polar sun synchronous orbit. When the PSLV became operational, ISRO agreed to accommodate the proposed Indian X-ray Astronomy Experiment (IXAE) to be flown on the Remote sensing satellite IRS-P3. Four argon-filled proportional counters (area $\sim$1600 sq cm) and the front end electronics was designed and provided by the TIFR group and the ISAC group designed and supplied the signal processing electronics (Agrawal *et al.* 1997). Developed in a record time of 18 months, this instrument named as Indian X-ray Astronomy Experiment (IXAE), was launched on March 21, 1996 in a polar orbit by the PSLV. Using a star sensor the IXAE detectors were pointed towards the sky for about 2 months every year to study specific sources. The IXAE performed well for about 5 years and studied about 20 X-ray sources. This experiment produced many new results especially on a new transient black hole binary GRS 1915+105 (Paul *et al.* 1998). The success of the IXAE was a major milestone in the evolution of the idea of AstroSat as it gave confidence that Indian scientists can make the gas filled detectors that can work in space (Agrawal 2017). One of the scientists associated with the IXAE proposed to ISRO a dedicated Indian X-ray astronomy satellite with a more complex and heavier X-ray experiment which will lead to internationally competitive science. ISRO suggested expanding the scope by convening a meeting of Indian astronomers where this and other proposals were further deliberated, for a dedicated astronomy mission.

2. AstroSat

This is the golden age for multi-wavelength astronomy. Ground-based optical telescopes have extended to tens of meters in size, radio astronomy telescopes extending their capabilities to long wavelengths, huge arrays and improving the spatial resolution with interferometry, new facilities like mm wave astronomy making a mark and a large number of space astronomy satellites covering almost the entire wavelength range from optical to high energy gamma rays. These have been made possible by the aspirations of the scientists world over to continuously improve on the capabilities and broaden and sharpen the knowledge base already achieved.

The success of the GRB and the IXAE propelled a series of meetings of the Indian astronomical community to explore the possibility of a major Indian astronomical observatory in space. By mid 1990s, NASA's Hubble Space Telescope and CGRO were already operational in orbit and the Chandra X-ray mission and ESA's XMM-Newton were well into final stages of development. Even more ambitious missions were being funded or under planning world over. Given this international scenario, and the proven capabilities and resources within India, the critical question was to ask "What should be the nature and scope of the Indian mission?"

Traditionally, the quest for higher sensitivity and higher angular resolution has been the motivating factor for newer missions. It became clear from the discussions that this is not the only goal we could aim for. Indian astronomers worked towards defining a mission that could, while supplementing other missions, have its own niche objectives which would encompass the research interests of the scientific community and technical capabilities of the engineering teams within the country.

The final consensus was a multiwavelength astronomical observatory, based on the following reasoning. To understand the nature of cosmic sources, their radiation processes and environment, it is necessary to measure their emission over a wide range of the electromagnetic spectrum. Since intensity of several classes of cosmic sources varies with time, it is necessary to make simultaneous observations in different wavebands. Most of the space observatories are dedicated to a particular waveband, e.g. X-ray, UV etc. Consequently, multiwavelength studies usually have to be made from coordinated observations with different satellites. Often there are logistic problems in making simultaneous and coordinated studies of a specific object from different satellites and ground based telescopes. The most efficient and effective way to pursue multiwavelength studies is to have a dedicated satellite mission which will carry several instruments covering the desired spectral bands so that simultaneous observations in all the desired wavebands can be made from the same satellite.

There are however, different observational constraints for instruments operating in different wavebands and therefore it was also decided that the scientific objectives could include some specific aims which could also be realized using individual instruments/wavebands.

2.1 *Objectives*

The AstroSat was therefore proposed as a multiwavelength astronomy mission with wide spectral coverage extending over Near and Far Ultraviolet (NUV, FUV), soft and hard X-ray bands (Agrawal 2006; Rao *et al.* 2009).

It has provided an opportunity to astronomers to carry out cutting edge research in the frontier areas of X-ray astronomy and Ultraviolet astronomy and allow them to address some of the outstanding problems in high energy astrophysics.

The scientific objectives of AstroSat are the following:

(1) Understand high-energy emission processes in various astrophysical systems: Multiwavelength studies of various cosmic sources over a wide spectral band extending over visible, UV and X-ray bands.
(2) Correlated time variations of intensity in UV, soft and hard x-ray bands to investigate the origin and mechanism of the emission of radiation in different wave bands.
(3) Understand variability, timescales in various astrophysical systems through broad-band and long-duration observations: studies of periodic (pulsations, binary light curves, QPOs etc.) and aperiodic (flaring activity, bursts, flickering and other chaotic variations) variability.
(4) Search for black hole sources by limited surveys in galactic plane; detection and detailed studies of stellar-mass black holes.
(5) Study of non-thermal emission in supernova remnants and galaxy clusters.

(6) Study magnetic fields in strongly magnetized systems: Measuring magnetic fields of neutron stars by detection and studies of cyclotron lines in the X-ray spectra of X-ray pulsars.
(7) Detection of X-ray transients and long duration temporal studies.
(8) High-resolution UV studies of stars, emission nebulae and galaxies: study of UV emission from hot stars (WD, CV, WR, LBV, β-Cephei, etc.) in galaxies, morphological studies of nebulae and supernova remnants and nearby galaxies.
(9) Limited sky survey in UV: multi-band limited sky survey in ultra-violet in 130–300 nm band.

To accomplish the above scientific objectives, the instrument configuration was flown as a combination of four types of X-ray detectors and twin telescopes covering visible, NUV and FUV bands (Singh *et al.* 2014; Agrawal 2017). The instrumentation flown had the following features:

- Large Area X-ray Proportional Counters (LAXPC) (3 nos) to cover the energy range 3–80 keV, and to have an effective area of $\sim$6000 cm^2 at 15 keV and a time resolution of 10 microsecond (Agrawal *et al.* 2017; Yadav *et al.* 2017).
- Twin Ritchey Chretian UV Imaging Telescope (UVIT) covering the wavelength band of 130–180 nm and 200–300 nm (using several filters) and having an angular resolution better than 1.8 arcsec (Tandon *et al.* 2017).
- Soft X-ray Telescope (SXT) covering the energy range of 0.3–8 keV with an angular resolution of 3–4 arcmin (Singh *et al.* 2017).
- Pixellated Cadmium Zinc Telluride Imager (CZTI) operating in the energy range 20–100 keV with an area of 1000 sq cm, with a collimator and coded mask. Above 100 keV, it operates as a detector without collimation (Bhalerao *et al.* 2017a, b).
- Scanning Sky Monitor (SSM) operating in the X-ray range of 2.5–10 keV, with a one-dimensional coded mask (Ramadevi *et al.* 2017).
- A Charge Particle Monitor (CPM) capable of detecting protons >1 MeV (Rao *et al.* 2017).

Design and fabrication of three of the X-ray astronomy instruments namely LAXPC, SXT and CZTI and the CPM were the responsibility of TIFR, and the responsibility for UVIT was with the Indian Institute of Astrophysics, (IIA) and the SSM instrument by ISAC. Figure 1 is a collage of the flight models of the main five payloads and in the center is the picture of assembled satellite on ground.

The realization of the above instruments was made possible with the involvement of many institutions in addition to various Centres of Indian Space Research Organisation (ISRO). They are Tata Institute of Fundamental Research (TIFR), Mumbai, Indian Institute of Astrophysics, (IIA) Bengaluru, Inter-University Centre for Astronomy and Astrophysics, (IUCAA) Pune, Raman Research Institute, (RRI) Bengaluru, Physical Research Laboratory, (PRL) Ahmedabad along with a collaboration with Canadian Space Agency for the detectors and electronics of UVIT and with University of Leicester, UK for the detectors of SXT.

There were several challenges in realizing the payloads and the satellite, a few of them being:

- Achieving an overall angular angular resolution of <1.8 arc-sec for the UVIT telescope with a field-of-view of 28 arcmin, with indigenous development of UV mirrors for the first time.
- Development and testing of indigenous gold-coated foil optics for soft X-ray telescope, and ensure an aligned assembly of these mirrors.
- Development of large high pressure gas filled counters with effective area $\sim$6000 cm^2 with energy measurement up to 80 keV, and a temporal resolution of 10 microsecond. A major challenge in the LAXPC instrument was also to develop a light weight multi-layer collimator yet opaque to X-rays up to 80 keV.
- Qualification of position sensitive gas-filled counters and rotation mechanism for SSM.
- Qualifying of commercial Cadmium Zinc Telluride detectors for astronomy purposes, and demonstrating the polarisation capabilities of CZTI.
- Contamination control of UVIT optics.
- Development of doors for the UVIT and SXT, and deployment mechanism.
- Capability for large onboard data storage with read/write capability.
- Inter-payload alignment and measurement on ground and measurement after launch using celestial sources.
- S/C maneuvering with avoidance of the Sun along two axes, and S/C pointing and stability.
- Enabling data storage in photon counting mode for the payloads.
- Background simulations, estimate and modeling for the various detectors.

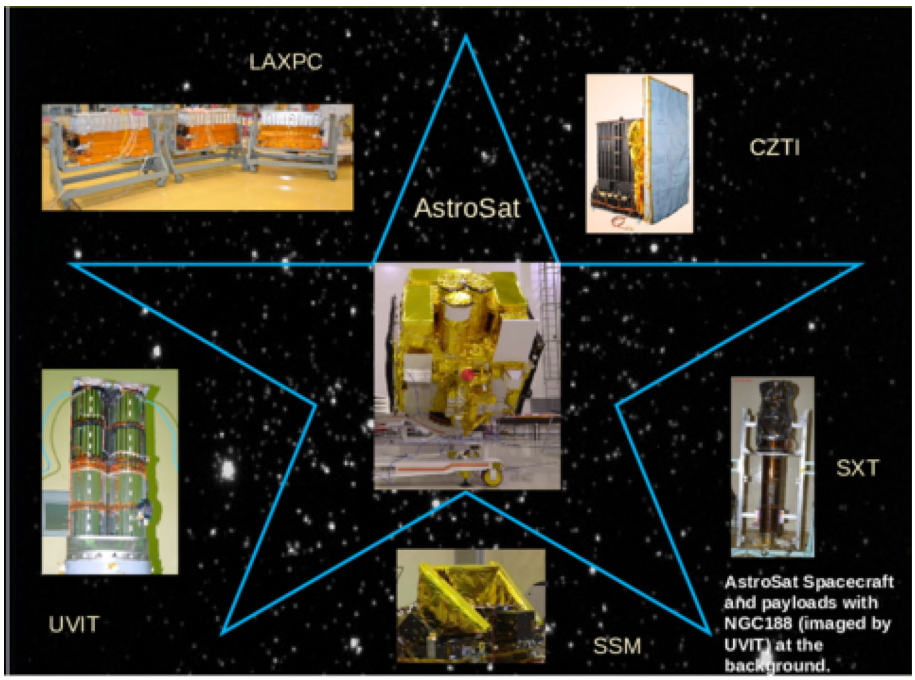

Figure 1. The five main payloads of AstroSat, and the assembled satellite in the centre, before launch. Image Courtesy: Payload and project teams and S. Megala.

It may be noted here that while the Neil Gehrels Swift Observatory and XMM-Newton do have capability to observe in NUV bands in addition to X-ray band. However they do not have FUV capabilities. On the other hand, the Hubble Space Telescope has extremely good resolution in Far UV, but over a narrow field-of-view. The advantage of UVIT is it can observed faint objects with $\sim$1.5 arcsec resolution with an FoV of nearly 0.5 degree, ideal for imaging galaxies. UVIT also has about 3 times better angular resolution than the earlier GALEX mission.

LAXPC with its large area of 3 counters enabled an effective area of LAXPC is $\sim$6000 sq cm at 15 keV (Antia *et al.* 2017). Above 30 keV, the effective area of the 3 LAXPCs together was four to five times greater than that of the Proportional Counter Array (PCA) on Rossi X-ray timing Explorer (RXTE).

2.2 *AstroSat mission management*

AstroSat with a mass of 1513 kg and a payload mass of 855 kg (Navalgund *et al.* 2017) was launched on 28 September 2015 by the Polar Satellite Launch Vehicle, PSLV-XL C30, into an orbit with inclination of 6 degree and an altitude of 650 km. This was the first time the payload mass was >50% of the satellite mass on an Indian satellite launched by PSLV. The inclination of the orbit was chosen to avoid the satellite traversing through the inner portions of the South Atlantic Anomaly region with high count rates of charged particles. The altitude was chosen to minimise the effect of atomic oxygen on the UVIT optics. This was also the first time PSLV launched a satellite in a low Earth orbit at a near equatorial inclination.

Four of the payloads namely the LAXPC, SXT, UVIT and CZTI have their view direction aligned to the +ve roll axis of the satellite (see Fig. 2). These payloads therefore are pointed towards the same source for observation. The sky monitor is pointed in a perpendicular direction and is rotated in a step and stare mode to scan as much of the sky in a rotation. For further details of pointing and maintenance of orbit, see Seetha and Megala (2017) and other papers in this volume.

The satellite was operated for the first six months for performance verification of the payloads, and the next six months was guaranteed time (GT) for the instrument teams (Pandiyan *et al.* 2017). In ensuing years, the GT gradually reduced and the observing time was gradually made open to both Indian and later international astronomers too.

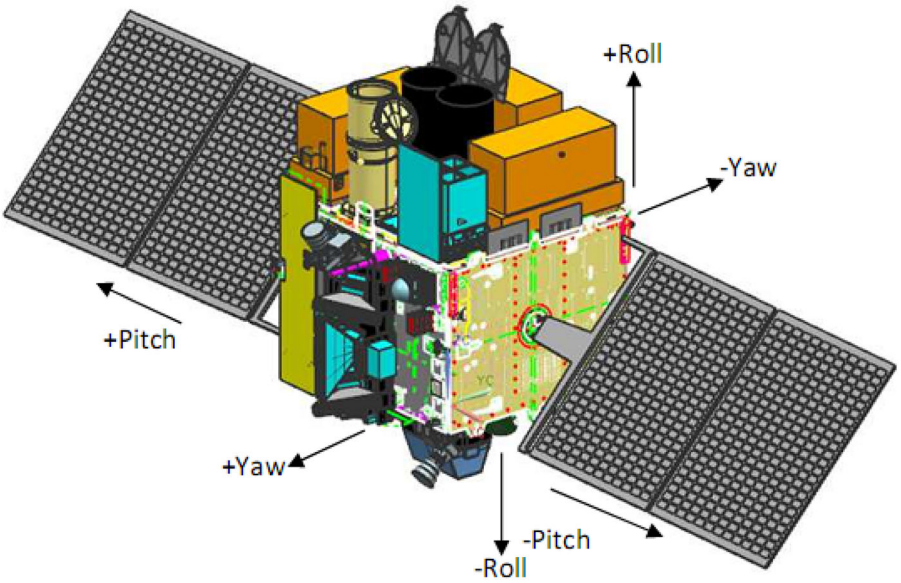

Figure 2. A drawing showing the post launch configuration of the payloads, with satellite axes reference. Image Courtesy: Project team.

2.3 *AstroSat as an Observatory*

AstroSat is operated as the first Indian Space Observatory. Observations are proposal driven. The AstroSat Proposal Processing System (APPS) is a web based software facility, developed through IUCAA, Pune, and hosted and administered by ISRO Space Science Data Centre (ISSDC), Bangalore. All proposal related activities like proposal submission, review, approval etc. are done through APPS. The call for proposals for observations are made through an Announcement of Opportunity (AO) typically issued in March of each year for an year's observation cycle starting from October. Announcement for various observations of Cycles are made by ISRO HQ in coordination with ISSDC and the Science Working Group (SWG). Proposals can be submitted by any scientist capable of utilising the data, with 55% of the available time being allotted for proposals from India. In addition to proposals for AO, proposals can be submitted anytime for Targets of Opportunity (TOO), (in case of any sudden outburst or state change to be observed in specific sources) and Calibration proposals (Cal). Submitted proposals are reviewed and approved through the APPS utility, by the AstroSat Time Allocation Committee (ATAC) for AO proposals, TOO committee for TOO proposals and Calibration Scientist for the Cal. Proposals. These committees are supported by recommendations by the AstroSat Technical Committee (ATC), which considers payload operation constraints like sun angle, avoidance of bright object, and sensitivity in the various instruments etc. Based on the approvals, the mission and operations team at UR Rao Satellite Centre, and ISRO Telemetry, Tracking and Command Network (ISTRAC) create the necessary list of targets to be observed, and generate command files, taking into consideration Sun avoidance, RAM angle constraints, data readout capability and thermal constraints. The operations of the payload and spacecraft are commanded at ISTRAC. Data is received and data products are again generated at ISSDC, and verified through Payload Operation Centres (POCs) and further made available for dissemination to the respective proposal Principal Investigators (PI). The data of observation under AO proposals has a lock-in period of twelve months with proposal PIs, after which it is made available to the public as archival data. The TOO data do not have any lock-in period and is released to public, along with proposer. The observations of TOOs have to be scheduled by sliding/shifting the pre-planned observations. Both proprietary data (during lock-in) and archival data are hosted on https://astrobrowse.issdc.gov.in maintained by ISSDC at ISTRAC. Anybody can download data through this website after registering in APPS.

The AstroSat calibration database (CALDB) and other tools/software required for analysing the AstroSat data are hosted/linked at the AstroSat support cell (ASSC, http://astrosat-ssc.iucaa.in/) hosted by IUCAA Pune. ASSC team also provides assistance to proposers and conducts workshops for training users for

proposal preparation and data analysis. ASSC is supported by ISRO.

All developments of necessary tools for operating the AstroSat as an observatory has been done for the first time in India for a space mission, and modified versions could be used for future astronomy satellites.

In the last five years, over 150 refereed publications, have resulted based on observations from AstroSat.

3. Scientific outcome

In this section, we provide a brief overview of the scientific results from AstroSat. This is to highlight the uniqueness of AstroSat and is by no means exhaustive. The references provided are mainly those resulting from AstroSat observations, and therefore we request the reader to consider pursuing the paper with the references therein for a better understanding of the scientific contributions on the topic.

3.1 *Multiwavelength observations*

3.1.1 *Her X-1.* Her X-1/HZ Her an accretion powered pulsar is an ideal target for multi-wavelength observations, with optical radiation from the companion star, X-ray radiation from the inner parts of the disc and the accretion onto a magnetised neutron star and UV/EUV radiation from the disc and the X-ray irradiated portion of the optical companion viewable due to the very conducive edge on view of this binary system with an inclination of about 85 degree. In addition to the spin and orbital variations, the X-ray data of this binary exhibits a 35 day cycle with two bright states referred to as main ON, and short ON with OFF or low states in between. This variation is explained in terms of a precessing accretion disc.

Spectral Observations using SXT on AstroSat at Low and High state of Her X-1 is consistent with earlier observations and a precessing disc model (Leahy & Chen 2019). FUV emission from this source indicates a variability starting near orbital phase of 0.3. FUV emission is estimated from two components after ruling out other contributions (Leahy *et al.* 2020): (a) due to the disc emission and (b) due to emission from heated portion of the companion star HZ Her. The geometry of the system is modeled by including FUV data. The current FUV observations are commensurate with a thin disc which is tilted and twisted and does not require a thick inner disc, which was used to explain X-ray data. However since the emission mechanisms have to match both the orbital phase and the X-ray emissions over the complex 35 day cycle, more detailed observations of both UV and X-rays over the different phases of the 35 day cycle may be required to further refine the model.

Closer to the neutron star, the X-ray observations of Her X-1 exhibit a cyclotron resonance scattering feature (CRSF, or referred as cyclotron line) produced by resonant scattering of photons off electrons moving perpendicular to the magnetic field, as accreted material flows along the magnetic field lines onto the polar cap of the neutron star. In the case of Her X-1, the cyclotron feature has been observed around 35 keV. The cyclotron peak energy is positively correlated with X-ray luminosity of the source which is explained in terms of reduction of emitting region with increasing luminosity/accretion rate (Becker *et al.* 2012). The time variation of the cyclotron feature has been studied for over three decades using data from various satellites and the peak energy of this feature is found to vary from 35 to 44 keV. It was found to be $\sim$35 keV before 1991, and a high value of 44 keV was observed in 1993 and 1996. Subsequently, a gradual decrease with time of this value, with episodes of constancy have been observed. The variation with time has been explained in terms of formation of a mound on the polar cap and changes in magnetic field due to this formation (Staubert *et al.* 2016 and references therein). Detailed modeling using previous and AstroSat data and considering various scenarios has been done by Bala *et al.* (2020). The authors fit the data with variation in both luminosity and time. They find that the best-fit corresponds to a case for which there is no time dependence beyond MJD 54487. The variation due to both luminosity and time, has been explained with the modeling of the dynamical variation of a mound over the polar cap of the neutron star. There is continuous inflow of matter leading to formation of a mound on the polar cap due to accretion along the magnetic field lines, and outflow of matter leaking through the edges (Mukherjee & Bhattacharya 2012; Mukherjee *et al.* 2013a, b). While the mound is gradually growing in size to few tens of meter, the magnetic field strength shifts from the centre to the edges of the mound, hence exhibiting a decrease in field strength with height of the mound. This explains decrease in cyclotron energy with increasing mound height. When the inflow and outflow balance each other there can be a constancy of the energy of the

cyclotron feature. However if the mound reaches a critical height, which is estimated by the authors to be about 100 m for Her X-1, it is very likely that the instabilities in the mound can cause sudden increase in outflow, leading to a sudden collapse of the mound and increase in cyclotron energy like that observed between 1991–1993.

3.1.2 *Blazar RGB J0710+591.* One of the main objectives of AstroSat was to conduct simultaneous observations over a broad spectral band, to estimate the spectral energy distributions (SEDs) for different types of objects, thus enabling the identification of physical processes in these objects. Blazars are Active Galactic Nuclei (AGNs) which have jets beamed towards the observer. Blazars exhibit a double peaked SED, with the lower energy synchrotron peak in the radio-x-ray regime, and the high energy peak in the x-ray to gamma ray energy regime. The synchrotron peak in high-energy-peaked blazars (HBLs) typically lies in UV–X-ray energies. RGB J0710+591 is one such blazar which was observed with AstroSat in 2016. These observations indicate that the X-ray part of the SED is unusually curved and can be explained in terms of synchrotron emission from a non-thermal distribution of high energy electrons with a declining energy density around the peak (Goswami *et al.* 2020). Such electrons can be produced from a region where particles are accelerated under Fermi process and the radiative losses in acceleration site decide the maximum attainable Lorentz factor. The UV part of the spectrum appears to be of a different emission component than X-ray. When this SED is compared with the SED of the same source obtained in 2015, using data from SWIFT and NuSTAR satellites, it is found that while the UV part is only marginally different, the X-ray part of the SED is significantly different.

3.2 *Stars and stellar systems*

UV observations are extremely sensitive to blue objects which include early type stars, blue stragglers, planetary nebulae, white dwarfs etc.

3.2.1 *Globular clusters and open clusters.* For long, Globular Clusters (GC) were considered to be consisting of co-evolving stars with single age and composition. In the last decade, observations have shown globular clusters could contain stars of more than one population. Figure 3 shows an image of the globular cluster 5466. UVIT on AstroSat was used to explore if the blue objects in GCs showed any evidence of multiple populations. Stars corresponding to different branches have been identified in both NGC 1851 (Subramaniam *et al.* 2017) and NGC 2808 (Jain *et al.* 2019), and both show there are more than one population among the horizontal branch stars. Observations of NGC 1261 on the other hand, exhibits blue horizontal branch (BHB) stars in UV but the red horizontal branch is too faint (Rani *et al.* 2020). Analysis of four other globular clusters NGC 4147, NGC 4590, NGC 5053 and NGC 7492, yield $\sim$150 blue horizontal branch stars (BHBs), and $\sim$40 blue straggler stars (Kumar *et al.* 2019). The temperature distribution of the BHBs is bi-modal, indicative of two groups.

Blue straggler stars (BSS) are stars which are bluer than the other stars which have evolved off the main sequence in a stellar cluster. They have often been referred to as rejuvenated stars having gained mass through some process.

NGC 188 is an old (7 Gyr) open cluster with 20 identified BSS. One of the other candidates WOCS-5886, also a member of NGC 188 was observed in both NUV and FUV using multiple filters of UVIT on AstroSat. The UV observations indicate the presence of excess flux in the UV region as compared to a spectral fit for a single star. Based on a spectral energy distribution fitting with these observations combined with those from other satellites/observatories, WOCS-5886 a member of NGC 188 is now identified (Subramaniam *et al.* 2016) to be a binary consisting of BSS and a hotter, post AGB/HB star with temperature of the BSS being 6000 K and the temperature of the companion being 17000 K, clearly indicating mass transfer as the likely mode for formation of BSS. This system is the first of its kind to be found in an open cluster.

The next step was whether BSS-WD systems could be identified, with the expected luminosity of WD being lower. Detection of white dwarfs with masses $<0.4M_{\rm sun}$ indicates evolution in binary systems, as single star evolution would take longer than the age of the Universe. Detection of WD-BSS binaries would therefore provide evidence for mass transfer from the pre-WD to the BSS, thus providing a clue to the formation of both the individual stars.

UV observations with AstroSat have resulted in the detection of WD-BSS binaries in open cluster M67 (Sindhu *et al.* 2019; Jadhav *et al.* 2019) and globular cluster 5446 (Sahu *et al.* 2019).

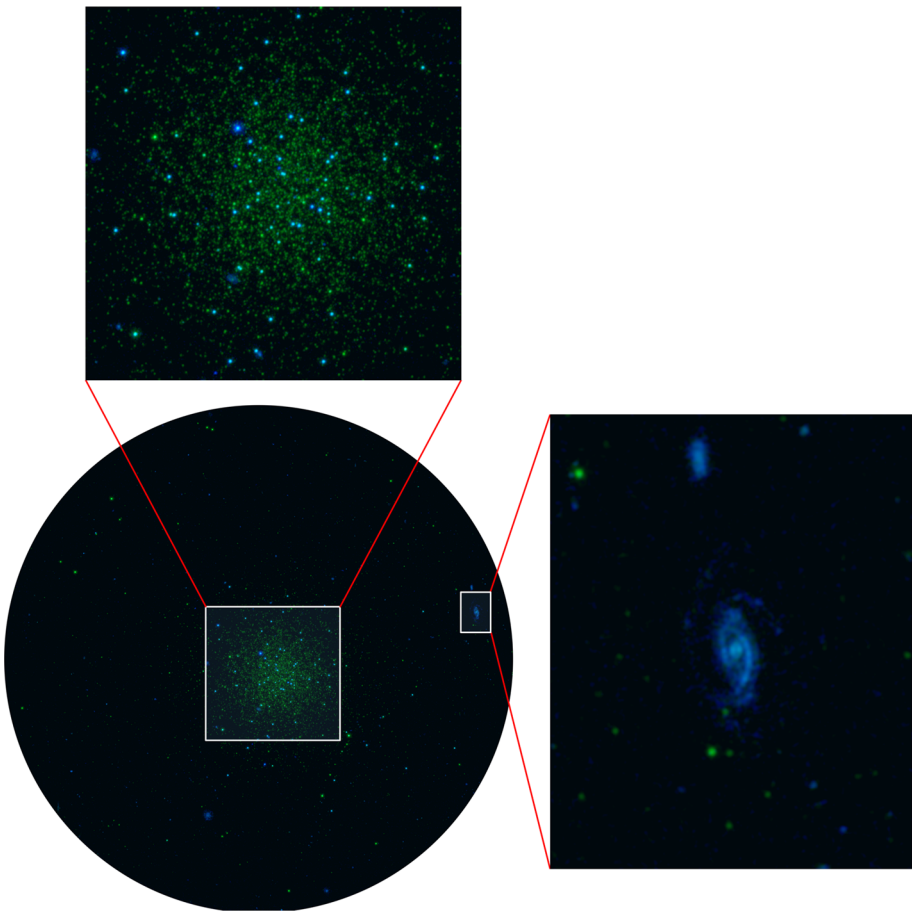

Figure 3. Image of the field containing globular cluster NGC 5466 observed with UVIT. Here, blue corresponds to observation with the F148W filter in the far ultra-violet (FUV) at a mean wavelength of 1481 Å, while green represents the observation with the N263M filter in the Near Ultra-Violet (NUV) at a mean wavelength of 2632 Å. Also shown are (i) expanded view of the cluster (top) and (ii) expanded view of a galaxy (right) that lies within the UVIT field. The exposure times in FUV and NUV are 5990 seconds and 8243 seconds respectively. Image Courtesy: UVIT, POC, IIA. For other AstroSat images and details, see outreach page of the Astronomical Society of India, https://astron-soc.in/outreach/apom/.

In the globular cluster 5446, NH84 has been identified to be a WD-BSS binary, the second such system in globular clusters, the first being in 47 Tuc.

Thirty stars have been studied in open cluster M67 (Jadhav *et al.* 2019), of which two have been identified as WD+BSS systems (WOCS1007, WOCS 2007), one as WD+yellow Giant and two WD+Main sequence binaries (see also Subramaniam *et al.* 2020). The BSS and the YG systems have extremely low mass WD (with mass $<0.3M_{\rm sun}$) as companion, clearly indicating their donor status. Figure 4 is a sketch of likely scenario of how BSS-WD binaries might have formed and evolve. The other systems studied include close binaries which could be progenitors of WD+BSS systems, and single WDs with masses $>0.5M_{\rm sun}$, which could in turn have formed from BSS as progenitors.

3.2.2 *Planetary nebulae.* NGC 40 or bow-tie nebula is a planetary nebula with a Wolf-Rayet star at its centre. For the first time a Far UV halo has been detected in the F169M sapphire filter of UVIT (Rao *et al.* 2018a). The FUV halo is most likely due to UV fluorescence emission from the Lyman bands of H_2 molecules, and trails the optical and IR halos, in the direction opposite to the central star's proper motion. NGC 6302 is another planetary nebula in which lobes are observed in the same FUV band (Rao *et al.* 2018b). The lobes are seen extending to 5 arcmin from the central hot and luminous bright object. In addition jets extending perpendicular to the line joining the lobes have also been observed.

3.2.3 *Flare stars.* The habitability of a planet not only depends on its location from the central star but

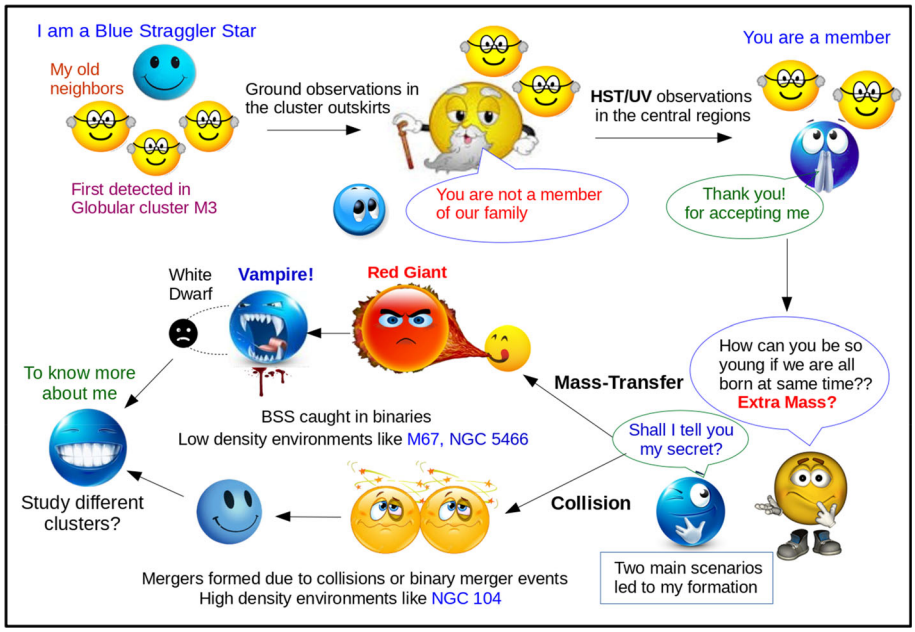

Figure 4. A sketch of the likely scenarios of formation of blue Stragglers, by the mass transfer pathway or the merger pathway due to collisions or binary mergers. The AstroSat findings of several white dwarf binaries including the extremely low mass white dwarfs in a binary system with blue stragglers suggest the mass transfer pathway for low density environments. Image courtesy: Snehalata Sahu.

also the environment it is exposed to. Activity on the central star can lead to mass loss from the planet's atmosphere. Proxima Centauri, the closest star to the solar system and also host to an Earth-like planet was observed by AstroSat, Chandra and HST to study the activity phase of this star. Flares have been observed in both X-ray and FUV observations from this star during 2017 (Lalitha *et al.* 2020). It is found that UV emission peak precedes the X-ray peak by 300–400 s. This could be due to the Neupert effect similar to that observed during some of the solar flares.

3.3 *Cataclysmic variables*

Cataclysmic Variables (CVs) are binaries with a white dwarf (WD) accreting matter from its companion, usually via the formation of an accretion disc, unless the magnetic field of the WD is sufficient to disrupt it. Novae form a subset of CVs. The accreted matter in novae increases in mass leading to explosive thermonuclear burning resulting in a nova outburst. Repeated outbursts are observed in Recurrent Novae (RNe), which could be progenitors for Type Ia supernovae. Of the confirmed RNe in our galaxy, four have red giants as companions similar to symbiotic stars and are referred to as Symbiotic Recurrent Novae. V3890 Sgr is one such symbiotic RNe which has so far exhibited two outbursts with a recurrence time of 28 years and hence it is a relatively rare event. The recent third outburst was during September 2019, observations of which were made in two slots with AstroSat (Singh *et al.* 2020). In the first slot between 8.1–9.9 days after outburst, the source initially exhibited a hard X-ray spectrum due to shock between nova ejecta and companion star, and on day 8.57, a super soft source (SSS) was evident in the spectra, the first view of the WD surface. The SSS was variable initially, but became brighter and stable after 8.9 day. The second slot of observation was from 15.9–19.6 d, with the source being brighter and variable, before fading away, with the SSS phase ending on day 26.18. The mass of the WD determines the duration of the SSS phase, with low mass WD having a longer phase, and indicates a high mass WD in V3890 Sgr. The source also exhibits temporary vanishing of SSS phase only re-appearing after a day, which could provide important clues regarding ejecta properties.

3.4 *X-ray binaries*

X-ray binaries are close binaries in which a companion star transfers matter to a compact star which could be a neutron star or a black hole. The primary goal for observations with the X-ray instruments on AstroSat

were to obtain high time resolution data on variability and broad band spectrum in X-rays, in order to understand the physical processes underlying these phenomena.

3.4.1 *Neutron star binaries.* The results on neutron star binaries can be divided into three parts: (a) broad band spectrum of Atoll and Z type sources which are Low Mass X-ray Binaries (LMXBs), (b) bursting sources which are also usually from LMXBs with neutron stars with relatively low magnetic field, and (c) accretion-powered pulsars and cyclotron lines usually from high mass X-ray binaries (LM × BS) and the neutron star has a magnetic field of $\sim 10^{12}$ Gauss.

3.4.1.1. Broad band spectrum of Z type and Atoll sources. GX5-1 a Z type source was observed with data on two branches in its hardness intensity diagram (HID). This was divided into 5 portions and analysed (Bhulla *et al.* 2019) The spectra could be fitted with a disc component rather than a black body component as was done in earlier studies and a thermal Comptonised component. This fit did not improve with inclusion of additional black body component. The low energy coverage with SXT, provides a better constraint on the column density. The disc flux to total flux changes monotonically from horizontal branch to normal branch, and disc flux itself is correlated to the disc flux ratio, indicating that disc flux ratio may be the component which places the source in a particular branch of the HID. Temporal analysis indicate a QPO $\sim$50 Hz, whose frequency increases from 30 Hz to 50 Hz while its rms decreases, with disc flux ratio.

On the other hand, LMC X-2 another Z type source was observed in 2016, and the source exhibited the complete Z pattern in the HID. The spectra were fitted with a Comptonization model alone and addition of a disk or a black body component, did not improve the fit (Agrawal and Nandi 2020). The authors therefore conclude that the disc if present is obscured by the Comptonisation region.

Data from atoll source 4U1705-44 (only LAXPC) in the banana state shows a significant flux component >20 keV and has been fitted with three different models. The authors find that a model with thermal Comptonisation + Gaussian for a broad iron line + non-thermal power-law fits the data best (Agrawal *et al.* 2018). The temporal analysis of various states of the banana state, also shows peaked noise features in the 1–13 Hz range, with most observations indicating a broad feature $\sim$10 Hz.

3.4.1.2. Bursting sources. A few neutron star low mass X-ray binaries also exhibit bursts. The bursts are considered to occur due to the thermonuclear burning of the accumulated accreted matter on the neutron star.

4U 1728-34 exhibited a burst during the observations in March 2016. Burst oscillations have also been observed during the rise portion of the burst, which is consistent with earlier burst oscillations (Verdhan Chauhan *et al.* 2017). This source also exhibited kiloHertz QPOs at 815 Hz, with an evolution to 850 Hz over a span of 3 ks of data. These QPOs are also observed >10 keV, for the first time with AstroSat. One of the outstanding issues in modeling bursts has been whether the pre-burst persistent emission spectrum can be considered non-changing and can be subtracted as background to estimate the burst spectrum. In order to assess this the burst data of 4U 1728-34 has been divided into smaller parts to study the evolution of the burst spectrum. This was made possible due to the large area of LAXPC, providing at least 5 bins with sufficient count rates. Based on this analysis it is found that the persistent emission does get enhanced and it is due to the burst emission possibly increasing the disc emission by increasing the accretion rate (Bhattacharyya *et al.* 2018).

Another bursting source 4U 1636–536 revealed the presence of a rare triplet of X-ray bursts, having gaps of few minutes between them. Though bursts with small gaps have been reported in few other sources, these LAXPC observations is shortest triplet with gap between first and second burst being 7 min, and with gap between second and third burst being 5.5 min (Beri *et al.* 2019). Since bursts occur due to thermonuclear burning, this time gap along with the state in color–color diagram and absence of mHz oscillations have to be taken together to constrain models for short recurrence time bursts.

The source 4U 1323-62 has been observed with LAXPC during February 2017, and during two days of observation six thermonuclear bursts were detected (Bhulla *et al.* 2020). The recurrence time between three consecutive bursts were found to be $\sim$2.66 hr. Rise time of the bursts were typically 10 s and total duration being 75 to 100 s. The bursts are detected only up to 20 keV and energy-dependent profiles of the bursts indicate they have maximum peak counts and last longest for the 3–6 keV range. A QPO is detected $\sim$1 Hz. Based on spectral modelling, a photospheric radius of 94–40 km is estimated assuming isotropic emission of burst.

3.4.1.3. Cyclotron lines and accretion powered pulsars. The detection of cyclotron resonant scattering feature (CRSF) has been observed at 5 keV in SXP 15.3 (Maitra *et al.* 2018) indicative of a magnetic field of 6×10^{11} G and is the second pulsar in small Magellanic cloud after SMC X-2 with a cyclotron line detection, and hence a confirmed magnetic field strength of the neutron star. The CRSF centroid energy varies with pulse phase, with an increase in energy and spectral hardening during an intensity dip. The characteristics mentioned above and the double-peaked pulse profile of SXP 15.3 indicate a fan-beam like geometry dominating the emitting region as is expected for super-critically accreting sources.

Two other wind fed pulsars sources in which cyclotron features have been detected are 4U1907+09 at 18.5 keV (Varun *et al.* 2019a), and 4U 1538–522 at ~22 keV (Varun *et al.* 2019b). An energy-resolved pulse variation has been observed up to 60 keV in both these pulsars. Energy-dependent pulse profiles are also found in 4U1909+07, but with no cyclotron feature (Jaisawal *et al.* 2020).

Be/Xray-binaries are binaries with a highly elliptical orbit and X-ray emission occurs when the neutron star is close to the periastron, and it accretes matter from the circumstellar disc of its companion Be star. This sudden increase in X-ray intensity is often observed as an outburst. The Be/X-ray binary GRO J2058+42 exhibited an outburst in April 2019, a part of which was observed by AstroSat (Mukerjee *et al.* 2020). Spectral analysis led to detection of three absorption features around ~10 keV, 20 keV and 38 keV. Magnetic field strength of 1.21×10^{12} Gauss has been estimated for the cyclotron feature at 10.81 keV. A QPO at 90 mHz and its harmonics, were also observed for the first time, indicative of formation of a transient disc during the outburst. The spin period of 194.22 s and the spin derivative are similar to that observed earlier using BATSE data.

Another Be/X-ray binary 3A 0726–260 (4U 0728–25) has been observed with AstroSat during 2016 (Roy *et al.* 2020). X-ray pulsations are observed from 0.3 keV to 40 keV at a period of 103.144 ± 0.001 s using both SXT and LAXPC. The period is detected above 20 keV for the first time. Pulse profile changes from single-peaked at lower energies to double-peaked at higher energies. Spectral-fit components include a broad iron line in addition to a power law with high energy cutoff.

3.4.1.4. Ultraluminous X-ray sources. Ultra-luminous X-ray sources (ULXs) are X-ray binaries with luminosities $\geq 10^{39}$ erg/s beyond the Eddington limit for a typical neutron star/black hole. Many of these are extragalactic and considered to be candidates for intermediate mass black holes.

With AstroSat two ULXs have been observed, both being Be/X-ray binaries with neutron star companions.

RX J0209.6−7427 a source discovered by ROSAT went into type II outburst in 2019, after about 26 years. Type II outbursts are much brighter and rarer than the type I bursts (caused during periastron passage of neutron star). The exact cause of these bursts are not fully understood and are probably due to sudden mass eruption from the Be star or due to accretion from the warped disc of the Be star which does not lie in the orbital plane of the binary system.

AstroSat observations of this 2019 outburst extends for the first time pulse profile observations beyond x-ray energies of 12 keV (Chandra *et al.* 2020). The pulse period is found to be 9.28204 s. and the profiles are similar in the 3–80 keV range, with pulse fraction being maximum in the 12–20 keV range. Spin up rate of 1.75×10^{-8} s/s estimated using LAXPC data, is much higher than the usual 10^{-11} s/s observed in pulsars. The rapid spin-up is indicative of accretion disc which is likely rotating in the same direction as the neutron star. Spectra of both SXT and LAXPC data in the energy range 0.5 to 50 keV, is fitted with a highly absorbed power law with a high energy cutoff and an Fe$^-$L Gaussian feature at 0.88keV. An X-ray flux of $3.7 \pm 0.1 \times 10^{-9}$ erg cm^{-2} s^{-1} which implies X-ray luminosity to be $1.6 \pm 0.1 \times 10^{39}$ erg/s for a distance of 60 kpc for the source. This pulsar may be an ULX located in the Magellanic Bridge in the vicinity of SMC.

The second ULX is Swift J0243.6+6124 a new transient discovered in October 2017. It was observed with AstroSat on 7th October (Obs-1) and 26th October 2017 (Obs-2) (Beri *et al.* 2020). Both the observations are during the rise of the outburst, with obs-2 being brighter than obs-1. Pulsations are detected at a period of 9.850 s in both the observations, in the energy range 0.3 to 150 keV (including CZTI observations up to 150 keV in Obs-2). The pulse profile in this source is double-peaked and shows a complex structure <7 keV in Obs-1. Pulse profiles of both observations are energy-dependent with pulse fractions increasing with energy. The luminosities estimated based on a spectral fit were found to be sub-

Eddington ($L_X \sim 7\times10^{37}$ erg/s) for Obs-1 and super-Eddington ($L_X \sim 6\times10^{38}$ erg/s) for Obs-2.

No cyclotron feature has been detected in both these sources, although strong magnetic fields are estimated by other methods. Observations of these two pulsars are important for future studies.

3.4.2 *Black hole binaries*

3.4.2.1. Mass and spin parameter. Black hole X-ray binaries are often observable only during an outburst, as the number of persistent black hole binaries is very small. In addition, during an outburst, the source may exhibit several spectral states. The mass and spin are fundamental parameters of a black hole. One method of estimating the spin, is by fitting the redshifted iron line in the spectra of black holes. The other method is by fitting the continuum spectrum, when the X-ray emission from the source is in a disc dominated high soft state, and the disc is expected to extend to the innermost stable circular orbit (ISCO).

4U1630-47 was observed to be in outburst mode in 2016. Observations in October 2016 indicated the source was in soft state during which the spectra could be fitted with primarily a disc spectrum. Chandra data and AstroSat data were obtained and analysed (Pahari *et al.* 2018a, b). This is the first time spectral fit in high soft state of 4U1630-47 has been used to estimate the spin to be 0.92 with over 99% confidence. In addition evidence of lines due to wind has also been found using Chandra data.

The same source was observed during both the (2016) and (2018) outbursts and spectral data using both SXT and LAXPC was analysed over the energy range 0.7–20 keV (Baby *et al.* 2020). The authors estimate the mass limits of the compact object using three methods to be 3–9 solar mass.

In GRS 1915+105, QPOs are detected in the range 3-5 Hz (Misra *et al.* 2020). Joint SXT and LAXPC spectral data are fitted with Kerrd model providing inner radius and accretion rate. Results show that the combined effect of QPO frequency and accretion rate have to be considered for finding the correlation with the gravitational radius. The QPOs are identified to be due to the general relativistically modified sound speed from the inner disk. The spin parameter is estimated to be 0.973+/–0.002.

During observations in 2017, the source exhibits high-frequency QPOs which varies from 67.4 and 72.3 Hz (Belloni *et al.* 2019). The centroid frequency of the QPO is also found to show a variation along the hardness intensity diagram, the frequency increasing with hardness. During these observations the source is predominantly in a disc dominated state, and the hard photons >10 keV lag with respect to soft photons. For the first time such small variations ($\sim$7%) in centroid frequency and time lags have been correlated with other parameters like hardness, though they are not sufficient to draw any new conclusions.

3.4.2.2. Black hole binaries with high mass companion. Cyg X-1 was studied in its hard state during January 2016 and found to have a predominantly thermal Comptonised fit (Misra *et al.* 2017). In the hard state, the overall understanding is, the disc is truncated at a radius far out from the ISCO. The seed photons from the disc are Comptonised in a region which lies inward of the truncated radius, and occasionally can also lead to a reflected component in the form of an iron line. The temporal spectrum exhibits two broad peaks at 0.4 and 3 Hz. It is found that there is a lag of the high energy photons, in the range 20–40 keV with respect to the low energy photons of 5–10 keV, which varies as a function of frequency and decreases from 50ms at lower frequencies to 8 ms at 2–5 Hz frequency.

Further analysis of more data sets of the same source in hard state are done, and it is found that the power density spectrum (PDS) exhibits two broad peaks for January 2016 data set and three broad peaks in the other five data sets (Bari *et al.* 2019). The large energy coverage of LAXPC and the time resolution allows for studying the frequency and energy dependence of the rms and the time lag of the hard photons based on a stochastic propagation model. The power density spectrum (PDS) of black hole binaries exhibit broad continuum noise-like features, which could be due to perturbations occurring in the disc. The energy-dependent variability in these features of the continuum observed in many black hole binaries, is explained in terms of propagation of perturbations from the outer regions of the disc, all the way to the inner regions. Bari *et al.* (2019) explain this and the frequency dependence of the time lags, by considering the inner Comptonisation region to be a single temperature, optically thin, geometrically thick disc, instead of multiple Comptonisation regions. The frequency-dependent time lag between different energy bands may be due to an underlying time lag between seed photon fluctuations and subsequent variation of heating rate of the hot inner flow.

Cyg X-3 is an X-ray binary with an estimated mass $2.4M_{\rm sun}$ for the compact object, which could either be a neutron star or a black hole. However, broadband

spectral properties favour a black hole. Cyg X-3 exhibits an asymmetric orbital modulation of $\sim$4.8 hr, which is attributed to periodic covering of the compact object by a plasma cloud.

Radio jets have been observed in several X-ray binaries and the connection between the X-ray emission and radio flaring has been an interesting problem in recent years. This phenomenon can be well studied during an outburst and also in bright persistent sources. Cyg X-3 had an outburst in 2017, and it was observed using SXT and LAXPC on April 1-2, during which the X-ray source was caught displaying spectral state transition, coincident with a rise of radio flux (Pahari *et al.* 2018a, b). The initial 10–12 hours of this observation was modelled with a disc spectrum and a Bremsstrahlung to account for the wind fed by the companion star. This state has no significant photons >17 keV and is termed as hypersoft state (HPS). The source then becomes more luminous with the spectrum having an additional hard component modelled by a power law with a photon index of $\sim$1.49, termed as Very High State (VHS). The authors find that during this intensity and spectral transition the radio flux intensity at 11.2 GHz using RATAN-600 radio telescope increases from 100 to 476 mJy. In addition it is found that while the 3–6 keV count rate is strongly correlated during the HPS with the 15–60 keV count rate with the Spearman Rank Correlation Coefficient (SRCC) of 0.82, it reduces to 0.17 during VHS. The hard component is therefore attributed to a different origin, and when the power law is extrapolated to radio frequencies, it matches the radio flux intensity levels. Hence the power law emission is attributed to synchrotron emission from the slowly moving radio jet base. This is supported by the fact that the temperature of the inner disc reduces and the radius increases indicative of receding of the disc with formation of a central blob of plasma.

The data obtained with AstroSat (SXT and CZTI) in 2015, when combined with $\sim$45 years of archival data exhibits a simple secular variation of the binary period, without any second derivative (Bhargava *et al.* 2017). Small variations are however indicated, most likely associated with jet emission.

Data has been collected on this source intermittently for over a year from October 2015, and exhibits different spectral states. In addition to orbital variations, a likely period around 35.8 days is detected (Pahari *et al.* 2017). During the flaring hard X-ray states and only rising phases of orbital modulation, a QPO of $\sim$20 mHz is observed. The fractional RMS of the QPO tends to show an increasing trend with energy, and a soft lag (soft photons lagging hard photons) of few seconds is observed. The rising portion of the orbital modulation is when the accreted material is high in this wind fed binary. The origin of the QPO and soft lag is therefore attributed to accretion of oscillating clumpy material, with the amplitude of the oscillations being boosted by in-phase oscillation of the material of the corona, with Compton down scattering of the hard photons.

3.4.2.3. Transients. MAXI J1535-571 is an X-ray transient discovered in 2017. Observations using AstroSat were done when the source was in hard intermediate state. The source exhibits $\sim$2Hz QPOs with change in QPO frequency from 1.85 to 2.88 Hz (Sreehari *et al.* 2019). The fundamental frequency at 2.21 Hz is observed in the energy range 3–50 keV while its harmonics are only detected at energies below 35 keV. Using the two-component accretion flow, the mass of the compact object is estimated to be in the range 5–7.8 solar mass. With a more detailed analysis of the QPO, it was found that the change in frequency is found to be correlated with power law index of the spectral fit but not with luminosity (Bhargava *et al.* 2019). Further, the wide band spectrum appears to be fitted best with a model of spinning black hole (Sridhar *et al.* 2019) which estimates the mass of the black hole to be $10.39\pm0.61 M_{\rm sun}$ and the dimensionless spin parameter to be 0.67.

Another new transient MAXI J1820+070 went into outburst in March 2018. AstroSat observations were made during its hard state and the spectra are fitted with a disc, thermal Comptonisation and reflection component. The hard X-ray component is believed to be from the regions inner to that of a truncated disc due to a Comptonisation region, with the seed photons being from the disc. A QPO is observed at 47.7 mHz and a likely one $\sim$109 mHz (Mudambi *et al.* 2020). In addition the continuum in the temporal Power Density Spectrum (PDS) can be fitted with 3 broad humps. The fractional RMS at a given frequency of the continuum decreases with energy and the time lag of hard photons with respect to the soft photons increases with energy. This energy and frequency dependence is explained in terms of the stochastic propagation model (Bari *et al.* 2019) in terms of propagation of perturbations from the outer regions of the disc, all the way to the inner regions. The perturbation time delay is of the order of 100 ms and is frequency-dependent, with the frequency dependence being similar to that of Cyg X-1.

3.5 *Galaxies and active galactic nuclei*

Dwarf galaxies are the most abundant type of galaxy in the universe. Many of them having been formed in the early Universe, they can provide important clues to the formation and evolution of galaxies. Star formation in these galaxies continue throughout cosmic time. Star formation in spite of their low metallicity and mass may indicate different pathways due to internal triggers like feedback from massive stars.

Wolf–Lundmark–Melotte, or WLM is an isolated irregular dwarf galaxy in the local group at a distance of 995 kpc. The UV emission extend to 1.7 kpc from the galactic centre, with FUV contour being smaller than NUV, which may be indicative of NUV emission from older stars compared to FUV emission (Mondal *et al.* 2018). The flux is mostly from the stars within a radius of 1 kpc. Multiple star-forming regions of temperatures >17500 K are observed with tens of regions with sizes 20–50 pc, and hundreds of regions with size <10 pc. Several hot regions have temperatures >35000 K indicative of O star population, and since their life time is 10 Myr, these regions may have formed recently. Star formation rate is estimated to be $0.008 M_{\rm sun}$/year. It is found that the hot regions are surrounded by cooler regions, indicating a clumpy nature, and possibly a feedback from the hotter regions triggering star formation in surrounding regions.

NGC 2336 on the other hand is a spiral galaxy viewed nearly face on, and hence ideal for studies of star forming regions (Rahna *et al.* 2018). 78 star-forming knots have been identified in the NUV band with 3 of them being in the inter-arm region and 6 of them being in co-rotation ring around the bar. Of these 57 knots are also identified in FUV. The knots have a mean size of 485 pc in FUV and 408 pc in NUV. The star formation rates vary from 6.9×10^{-4} to $2.2 \times 10^{-2} M_{\rm sun}$/yr in NUV and from 4.5×10^{-4} to 1.8×10^{-2} $M_{\rm sun}$/yr in FUV depending on the mass of the star-forming knots, with average being 4.7×10^{-3} $M_{\rm sun}$/yr in NUV and 4.1×10^{-3} $M_{\rm sun}$/yr in FUV. Using the FUV–NUV color, it is found that the blue knots are towards the centre. It is suggested that star forming is driven by spiral density wave.

The number of early type galaxies is found to grow due to merging of galaxies to form an elliptical galaxy. Tidal forces can expel large amounts of molecular gas into the intergalactic medium, which later condenses and triggers star formation. Study of star formation in the tidal tails of merging galaxies often resembles dwarf galaxies and are referred to as tidal dwarf galaxies and forms an interesting topic especially in low density environment. NGC 7252 (atoms for peace galaxy) is one such galaxy with the merger having started 600–700 Myr ago and is now observed with a single nucleus remnant, with two tidal tails. The central part also has young clusters of stars. UVIT observations of this galaxy is used to identify 7 star-forming regions in the tails (including two regions already known (George *et al.* 2018a). Star formation rates in the already known regions is found to be 0.02 and 0.03 $M_{\rm sun}$/yr, comparable to other dwarf galaxies. A weak dependence of star formation rate density is observed with distance from the centre, which could be indicative of initial conditions in the merger.

The central region of the galaxy has been studied in detail. Based on the FUV-NUV color a blue circum-nuclear ring of radius $10''$ with a radius core of $4''$ is detected (George *et al.* 2018b). The blue ring has stellar formation regions, and is comprised of stellar populations with ages ≤300 Myr, with embedded star-forming clumps of younger age (≤150 Myr and 250 Myr). The red core region is devoid of star formation and extinction being the cause of the color is ruled out based on ground-based observations. The authors suggest that this could be the result of a central black hole which could launch a jet and a blast wave from the jet can create a bow shock in the vertical direction, pushing the gas outwards creating a cavity at the centre thus suppressing star formation in the core. If a critical density is achieved in the outer regions, star formation can be triggered in the form of a ring around the core.

Jelly fish galaxies are another set of galaxies which exist in clusters and in which gas is stripped off due to ram pressure. The intra-cluster medium consists of hot X-ray emitting plasma. The interstellar medium of spiral galaxies, which usually exist in the outer regions of the cluster, start experiencing a force opposite to their orbital velocity as they fall into the intra-cluster plasma. This leads to ram stripping of gas which modifies the morphology and converts rich star forming galaxies to partial or fully gas stripped galaxies, and making them as passively evolving systems. The gas gets stripped and also undergoes shock compression, and therefore can be sites of star formation. Jelly fish galaxies, so named because of their appearance, can therefore have tentacles and still retain part of their spiral form, and are detected in H_α images.

JO201 is a jelly fish galaxy located in the Abell 85 cluster with a redshift of 0.056 with a corresponding luminosity distance of 250 Mpc. UV images of JO201

in Abell 85 cluster have been obtained using UVIT on AstroSat (George *et al.* 2018c). 89 star-forming knots are detected in NUV, of which 85 are confirmed with H_α images using the Multi-Unit Spectroscopic Explorer (MUSE) on the very large telescope (VLT) at ESO (Bellhouse *et al.* 2017). Of the 89 knots, 80 are confirmed based on redshift and extinction measurements of H_α. 24 knots are present on the disk and the remaining 56 are outside the disk within the intergalactic medium. Star formation rates (SFR) for the knots of the disc range from $\sim$0.05 to 2.07$M_{\rm sun}$/yr. The SFR of knots outside the disk has a median value of $\sim$0.05 $M_{\rm sun}$/yr and range from $\sim$0.01 to 0.6 $M_{\rm sun}$/yr. Further results indicate quenching of star formation in the central region close to the AGN and a region outside it with enhanced star formation providing evidence of feedback mechanism (George *et al.* 2019).

3.6 *Polarization*

The Cadmium Zinc Telluride Imager (CZTI) on AstroSat becomes a wide angle detector at high energies above 100 keV. This enables CZTI to detect GRBs, which can occur anywhere in the sky. This property of CZTI combined with the capability of the detectors to be able to detect Compton scattered X-rays in adjacent pixels of the CZTI has led to the detection of over 200 GRBs, and more important detect polarisation in some of these bursts. Polarisation studies began with detection and study of spin phase dependence of polarisation in Crab (Vadawale *et al.* 2018). Polarisation has been detected in many GRBs observed using CZTI (Chattopadhyay *et al.* 2019). Of these 5 of them have detection above 3 sigma. Polarisation studies can help in understanding the processes leading to GRBs. Recent spectropolarimetric studies of the prompt emission using AstroSat, Swift and Fermi data of GRB160325A, and afterglow measurements using Swift XRT/UVOT measurements have demonstrated this capability (Sharma *et al.* 2020). The afterglow observations indicate that the jet emission is pointed towards the observer. The spectra of prompt emission consisting of two episodes separated by 9s, has been modeled using the fireball model. The first of the two episodes is due to quasi-thermal Comptonisation in the photosphere, and the second episode, due to synchrotron emission produced in internal shocks in the optically thin region above the photosphere, and having high polarisation. CZTI observations have also been used to differentiate between the emission due to gravitational wave source GW 170104 and gamma ray burst source GRB170105A (Bhalerao *et al.* 2017a, b).

3.7 *Deep survey using UVIT*

3.7.1 *Andromeda galaxy.* Our neighbouring spiral galaxy M31 or Andromeda galaxy located at 783kpc has been studied in detail using the UVIT. The central bulge covered in 7 pointings of the galaxy is found to have 31 bright sources clustered around a central 5 arcmin. Radius around the nucleus (Leahy *et al.* 2018). SEDs are constructed for 26 of these sources along with the HST Panchromatic Hubble Andromeda Treasury (PHAT) covering the wavelength from 275 to 1600 nm in six bands. Most of the SEDs are double peaked, their fits indicative of a hot and cool star. The fit for hot stars correspond to main sequence (5–20$M_{\rm sun}$) and the cooler stars to giant branch.

Further observations of the galaxy with 18 pointings has resulted in a UVIT catalog of total of 74,907 sources identified in 4 FUV filters or 2 NUV filters, with largest number (31000) being in the CaF_2 filter of FUV having a bandwidth of 125–175 nm.

A matching is done with the UVIT source catalog and the Chandra catalog (Leahy & Chen 2020). Totally 67 sources are common in various bands. The UV and X-ray data are analysed using power law and black body models.

3.7.2 *Lyman continuum from z = 1.42 galaxy.* Observational evidence of star formation in distant galaxies, supporting the concept of the epoch of re-ionisation in the early Universe, is one of the interesting problems in astronomy. Detection of Lyman Continuum (LyC <900 Å) is an important marker indicating the escape of ionising radiation. Inter-galactic matter prevents direct observation of the LyC from very distant galaxies. Hence direct LyC observations can be made in UV for nearby galaxies $z < 0.4$. Observations of galaxies with $2.5 < z < 3.5$ is made possible as the LyC is redshifted to optical/IR bands. For this purpose, there has been a systematic study of deep fields both from ground- and space-based observatories. One of the goals of UVIT was also to conduct deep survey of specific areas in the sky. For this purpose, deep fields which had been surveyed by Hubble Space Telescope was chosen in order to maximise the scientific outcome from the observed celestial objects. One such field was the GOODS-South field observed using the UVIT

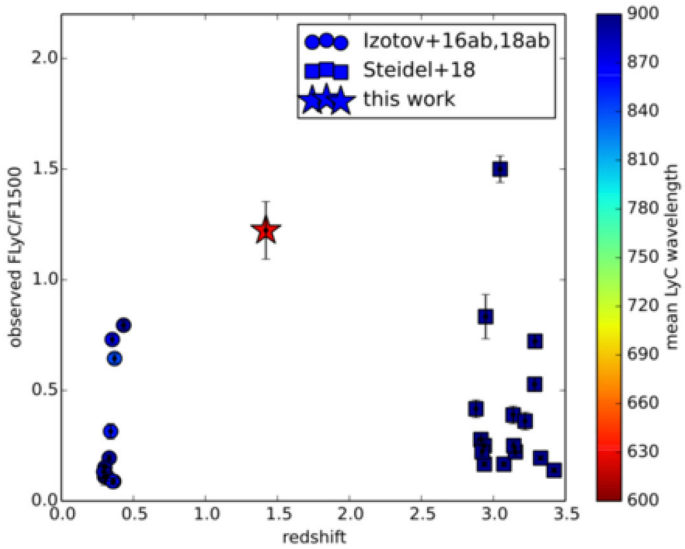

Figure 5. The LyC flux detected from different galaxies at different z. The red star at the centre is from Saha *et al.* (2020), indicating detection of rest frame EUV photons at $z \sim 1.42$. Image Courtesy: Kanak Saha.

instrument onboard AstroSat. From this field, the object AUDFs01 (AstroSat ultra deep field source 01) was chosen for in depth study (Saha *et al.* 2020) from the data of Hubble Extreme Deep field of HST. Based on HST data, it was identified to be a clumpy galaxy exhibiting broad and strong Hα and [OIII] lines and found to be at $z \sim 1.42$. The Lyman break wavelength corresponds to the NUV band of the UVIT for this redshift of $z = 1.42$, and a rest frame EUV wavelength ∼600 Å corresponded to the FUV band of UVIT. This object AUDFs01 was found have a good S/N in the UV bands of UVIT on AstroSat, and therefore enabled the detection of LymanC leakage from this source. This observation of the UV Imaging telescope of AstroSat, is made possible due to the reduced background of the UVIT detectors combined with the long exposure time. As to why only UVIT detected this galaxy in FUV, we quote the authors, 'one can also think that UVIT is more sensitive to low-surface-brightness objects because it has a lower spatial resolution and thereby samples more angular area per unit detector element.' This source AUDFs01 is classified as a clumpy galaxy with 4 clumps. The escape fraction of Lyman Continuum is estimated to be at least 20%, and is thus a good candidate of small faint galaxies providing ionising radiation, which could be an analogue for the Epoch of re-ionisation. This result is therefore the first detection of Lyman Continuum from a galaxy at $z \sim 1.42$, in the hitherto unexplored range of $0.4 < z < 2.5$, often referred to as the 'redshift desert' for LyC. Figure 5 shows the observed LyC fluxes of the detected galaxies from literature (Izotov *et al.* 2016a, b, 2018a, b; Steidel *et al.* 2018). It may also be mentioned that the observation of Saha *et al.* (2020) for the first time is from rest frame EUV photons (hence depicted as red star symbol), and this could provide crucial input towards questions such as: (a) at what redshift does the peak of star formation density occur? (b) does escape fraction of LyC evolve? Further detection of many more LyC galaxies are expected to provide answers to these outstanding queries.

4. Beyond AstroSat

Taking cognizance of the spectacular success of the AstroSat mission in terms of the basic concept, the configuration, a number of state-of-art scientific instruments backed up by a sophisticated highly maneuverable spacecraft with precision pointing capabilities and operating the spacecraft truly as an observatory in space, that have all together made India develop the full confidence in realizing an end-to-end astronomical observational space objective. The mission management including multiplicity of observers from different parts of the world placing their own demands on the observational time and the ability to realize the same by the mission management and ground system operations puts India among a select group of countries carrying out such a complex operation successfully.

The scientific outcomes already realized by AstroSat over the last five years add a wealth of knowledge in the field of ultraviolet and X-ray astronomy, including many new discoveries. This has spurred the Indian scientific community to plan immediately observatories such as XpoSat for X-ray polarization measurements and Aditya L1 for solar studies. Further, discussions are under way among the astronomical community to build a more ambitious AstroSat follow-on mission, that besides enhancing the capability of the ongoing spacecraft in the areas of ultraviolet, x-rays and gamma rays could have better sensitivity, more optimal choice of wavelength bands and much more sophisticated pointing and control system for the spacecraft. Needless to emphasize, the international collaboration and co-operation would certainly be a hallmark of such an ambitious astronomical space mission. The younger generation through AstroSat-1 have been trained, prepared and are confident enough to carry on its rich legacy.

Acknowledgements

We use the results of data from the AstroSat mission of the Indian Space Research Organisation (ISRO), archived at the Indian Space Science Data Centre (ISSDC). The authors wish to thank all the payload and project team members of AstroSat, and the authors of the scientific publications from AstroSat. The authors also wish to thank the reviewer for useful comments.

References

Agrawal P. C. 2006, Adv. Sp. Res. 38, 2989
Agrawal P. C. 2017, J. Astrophys. Astr. 38, 27
Agrawal V. K., Nandi A. 2020, MNRAS 497, 3726
Agrawal P. C., Paul B., Rao A. R. *et al*. 1997, J. Korean Astronom. Soc. 29, 429
Agrawal P. C., Yadav J. S., Antia H. M. *et al*. 2017, J. Astrophys. Astr. 38, 30
Agrawal V. K., Nandi A., Girish V. 2018, MNRAS, 477, 5437
Antia H. M., Yadav J. S., Agrawal P. C. *et al*. 2017, ApJS, 231, 10
Baby B. E., Agrawal V. K., Ramadevi M. C. *et al*. 2020, MNRAS, 497, 1197
Bala S., Bhattacharya D., Staubert R., Maitra C. 2020, MNRAS, 427, 1029
Bari M., Mudambi S. P., Misra R. *et al*. 2019, MNRAS, 486, 2964
Becker P. A., Klochkov D., Schönherr G. *et al*. 2012, A&A, 544, 123
Bellhouse C., Jaffé Y. L., Hau G. K. T. *et al*. 2017, ApJ, 844, 49
Belloni T. M., Bhattacharya D., Caccese P. *et al*. 2019, MNRAS, 439, 1037
Beri A., Paul B., Yadav J. S. *et al*. 2019, MNRAS, 482, 4397
Beri A., Naik S., Singh K. P. *et al*. 2020, MNRAS, 500, 565
Bhalerao V., Bhattacharya D., Vibhute A. *et al*. 2017a, J. Astrophys. Astr. 38, 31
Bhalerao V., Kasliwal M. M., Bhattacharya D. *et al*. 2017b, ApJ, 845, 152
Bhargava Y., Rao A. R., Singh K. P. *et al*. 2017, ApJ, 849, 141
Bhargava Y., Belloni T. M., Bhattacharya D., Misra R. 2019, MNRAS, 488, 720
Bhattacharyya S., Yadav J. S., Sridhar N. *et al*. 2018, ApJ, 860, 88
Bhulla Y., Misra R., Yadav J. S., Jaaffrey S. N. A. 2019, RAA, 19, 114
Bhulla Y., Roy J., Jaaffrey S. N. A. 2020, RAA, 20, 98
Chandra A. D., Roy J., Agrawal P. C. *et al*. 2020, MNRAS, 495, 2664
Chattopadhyay T., Vadawale S. V., Aarthy E. *et al*. 2019, ApJ, 884, 123
George K., Poggianti B. M., Gullieuszik M. *et al*. 2018a, MNRAS, 479, 4126
George K., Joseph P., Mondal C. *et al*. 2018b, A&A, 613, L9
George K., Joseph P., Côté P. *et al*. 2018c, A&A, 614, A130
George K., Poggianti B. M., Bellhouse C. *et al*. 2019, MNRAS, 487, 3102
Goswami P., Sinha A., Chandra S. *et al*. 2020, MNRAS, 492, 796
Izotov Y. I. *et al*. 2016a, Nature, 529, 178
Izotov Y. I. *et al*. 2016b, MNRAS, 461, 3683
Izotov Y. I. *et al*. 2018a, MNRAS, 474, 4514
Izotov Y. I. *et al*. 2018b, MNRAS, 478, 4851
Jadhav V. V., Sindhu N., Subramaniam A. 2019, ApJ, 886, 13
Jain R., Vig S., Ghosh S. K. 2019, MNRAS, 485, 2877
Jaisawal G. K., Naik S., Ho W. C. G. 2020, MNRAS, 498, 483
Kasturirangan K., Padmini V. N., Prasad N. L. *et al*. 1997, A&A, 322, 778
Kumar R., Pradhan A. C., Parthasarathy M. *et al*. 2019, in Bragaglia A., Davies M. B., Sills A., Vesperini E., eds, Star Clusters: From the Milky Way to the Early Universe, Proceedings IAU Symposium No. 351, 2019
Lalitha S., Schmitt J. H. M. M., Singh K. P. *et al*. 2020, MNRAS, 498, 3658
Leahy D. A., Chen Y. 2019, ApJ, 871, 152
Leahy D. A., Chen Y. 2020, ApJ Suppl. 250, 23
Leahy D. A., Bianchi L., Postma J. E. 2018, ApJ, 156, 269

Leahy D. A., Postma J., Chen Y. 2020, ApJ, 889, 131
Maitra C., Paul B., Haberl F., Vasilopoulos G. 2018, MNRAS, 480, L136
Misra R., Yadav J. S., Chauhan J. V. *et al*. 2017, ApJ, 835, 195
Misra R., Rawat D., Yadav J. S., Jain P. 2020, ApJ Lett. 889, L36
Mondal C., Subramaniam A., George K. 2018, AJ 156, 109
Mudambi S. P., Bari M., Misra R. *et al*. 2020, ApJ Lett. 889, L17
Mukerjee K., Antia H. M., Katoch T. 2020, ApJ, 897, 73
Mukherjee D., Bhattacharya D. 2012, MNRAS, 420, 720
Mukherjee D., Bhattacharya D., Mignone A. 2013a, MNRAS, 430, 1976
Mukherjee D., Bhattacharya D., Mignone A. 2013b, MNRAS, 435, 718
Navalgund K. H., Suryanarayana S. K., Gaurav P. K. *et al*. 2017, J. Astrophys. Astr. 38, 34
Pahari M., Antia H. M., Yadav J. S. *et al*. 2017, ApJ, 849, 16
Pahari M., Yadav J. S., Chauhan J. V. *et al*. 2018a, ApJ Lett. 853, L11
Pahari M., Bhattacharyya S., Rao A. R. *et al*. 2018b, ApJ, 867, 86
Pandiyan R., Subbarao S. V., Nagamani T. *et al*. 2017, J. Astrophys. Astr. 38, 35
Paul B., Agrawal P. C., Rao A. R. *et al*. 1998, ApJ Lett. 492, L63
Rahna P. T., Das M., Murthy J. *et al*. 2018, MNRAS, 481, 1212
Ramadevi M. C., Ravishankar B. T., Sitaramamurthy N. *et al*. 2017, J. Astrophys. Astr. 38, 32
Rani S., Pandey G., Subramaniam A. *et al*. 2020, accepted in MNRAS
Rao V. K., Agrawal P. C., Sreekumar P., Thyagarajan K. 2009, Acta Astronautica, 65, 6
Rao A. R., Patil M. H., Bhargava Y. *et al*. 2017, J. Astrophys. Astr. 38, 33
Rao N. K., Sutaria F., Murthy J. 2018a, A&A, 609, L1
Rao N. K., Marco D., Krishna S. *et al*. 2018b, A&A, 620, 138
Roy J., Agrawal P. C., Singari B., Misra R. 2020, RAA, 20, 155
Saha K., Tandon S. N., Simmonds C. *et al.* 2020, Nat. Astron., 24 August, https://doi.org/10.1038/s41550-020-1173-5, 2020NatAs.tmp..193S
Sahu S., Subramaniam A., Simunovic M. *et al*. 2019, ApJ, 876, 34
Seetha S., Megala S. 2017, Curr. Sci. 113, 579
Sharma V., Iyyani S., Bhattacharya D. *et al*. 2020, MNRAS, 493, 5218
Sindhu N., Subramaniam A., Jadhav V. V. *et al*. 2019, ApJ, 882, 43
Singh K. P., Tandon S. N., Agrawal P. C. *et al*. 2014, Proc. SPIE, 9144, 91441S
Singh K. P., Stewart G. C., Westergaard N. J. *et al*. 2017, J. Ap&A, 38, 29
Singh K. P., Girish V., Pavana M. *et al*. 2020, accepted for publication in MNRAS
Sinha S., Sreekumar P., Kasturirangan K. 2001, BASI, 29, 505
Sreehari H., Ravishankar B. T., Iyer N. *et al*. 2019, MNRAS, 487, 928
Sridhar N., Bhattacharyya S., Chandra S., Antia H. M. 2019, MNRAS, 487, 4221
Staubert R., Klochkov D., Vybornov V. *et al*. 2016, A&A, 590, A91
Steidel C. C., Shapley A. E., Pettini M. *et al*. 2018, ApJ, 869, 123
Subramaniam A. *et al*. 2020, this volume
Subramaniam A., Sindhu N., Tandon S. N. *et al*. 2016, ApJ, 833, 27
Subramaniam A., Sahu S., Postma J. E. *et al*. 2017, AJ, 154, 233
Tandon S. N., Hutchings J. B., Ghosh S. K. *et al*. 2017, J. Astrophys. Astr. 38, 28
Vadawale S. V., Chattopadhyay T., Mithun N. P. S. *et al*. 2018, Nature Astron. 2, 50
Varun B., Maitra C., Pradhan P. *et al.* 2019a, MNRAS, 484, L1
Varun B., Pragati P., Maitra C. *et al.* 2019b, ApJ, 880, 61
Verdhan Chauhan J., Yadav J. S., Misra R. *et al*. 2017, ApJ, 841, 41
Yadav J. S., Agrawal P. C., Antia H. M. *et al*. 2017, Curr. Sci. 113, 591